

# Titanium-alloy MEMS wing technology for a micro aerial vehicle application

T. Nick Pornsin-sirirak<sup>a,\*</sup>, Y.C. Tai<sup>a</sup>, H. Nassef<sup>b</sup>, C.M. Ho<sup>b</sup>

<sup>a</sup>Caltech Micromachining Laboratory, 136-93, Pasadena, CA 91125, USA

<sup>b</sup>Mechanical and Aerospace Engineering, University of California, Los Angeles, CA 90095, USA

## Abstract

In this paper, we present the first MEMS-based wing technology that we developed using titanium-alloy metal (Ti–6Al–4V) as wingframe and poly-monochloro-*para*-xylylene (parylene-C) as wing membrane. With this new MEMS wing technology, we are able to produce light, but robust 3-D wings, optimized to utilize the flow separation to achieve a high lift coefficient as large as five times that of the fixed-wing aircraft. The use of MEMS technology enables systematic research in terms of repeatability, size control, and weight minimization of the wings. We also constructed a high quality low-speed wind tunnel with velocity uniformity of 0.5% and speeds from 1 to 10 m/s. We have tested and have studied the unsteady-state aerodynamics of various types of MEMS-based and non MEMS-based wings. Finally, we built lightweight, palm-sized flapping-wing micro aerial vehicles (MAVs) with super capacitor-powered and battery-powered transmission systems and have demonstrated successful free flights with flight duration ranges from 5 to 18 s. © 2001 Elsevier Science B.V. All rights reserved.

**Keywords:** MEMS wings; Titanium-alloy; Parylene; MAV; Flapping-wing

## 1. Introduction

We started this project with two difficult constraints. The first constraint was that the flyer must be a MAV and, by definition, MAV must have a total wingspan less than 15 cm [1]. The second constraint was that the flyer must be an ornithopter (flapping-wing). It is interesting to note that 15 cm wingspan is the border between flyers capable of two different types of flight: most flyers smaller than this size are able to hover but cannot soar, while bigger flyers cannot hover but they can soar. We can see a great difference in the use of the wings and in the type of flight. For larger birds, the more common flight is soaring. Flapping is restricted to limited operations, such as take-off, landing, and stabilization. When soaring, the wings are used as fixed wings. For the smaller size of flyers, such mechanism is employed less. If we look at small birds and insects, such as swifts, hummingbirds, bees or flies, nature indicates that flyers of small sizes use the flapping-wing mechanism to generate lift to overcome their own weight. This mechanism is by far the most advantageous mechanism for flyers at these sizes when compared to mechanisms employing for fixed or rotating wings. One of the advantages is that

flapping-wing flight is much more efficient than fixed-wing flight when the size decreases. As shown in Fig. 1, the Reynolds number for MAVs and insects is in the range of 100–10,000. Airfoil performance of fixed-wing deteriorates severely for the Reynolds number at this range. The main effects are: (1) lower lift coefficient, which means lower loading capability; (2) higher drag coefficient, which means high power input; (3) flow separation on the wing, which means stall at low angles of attack, thus reduces the wing's performance and maneuverability. The conclusion is that the fixed wing is not as suitable for flight in this low Reynolds number regime compared to flapping-wing.

Presently, the aerodynamics of flapping-wing flight, especially for MAV size, is still not a fully explored subject. There have been studies of insect flights [2–4]; however, unlike the fixed-wing aerodynamics, there have not been any available design rules for flapping-wing aerodynamics for MAV size. As a result, we believe that there are two approaches for this project. One is to learn from natural MAV flyers and try to mimic them. The other is to study flapping-wing aerodynamics ourselves and try to improve them.

From our analysis of natural MAV flyers, we find that the MAV size falls within the range of small birds, bats, hummingbirds and other large insects [5]. Fig. 2 shows the plot of weight versus wingspan of some samples of

\* Corresponding author.

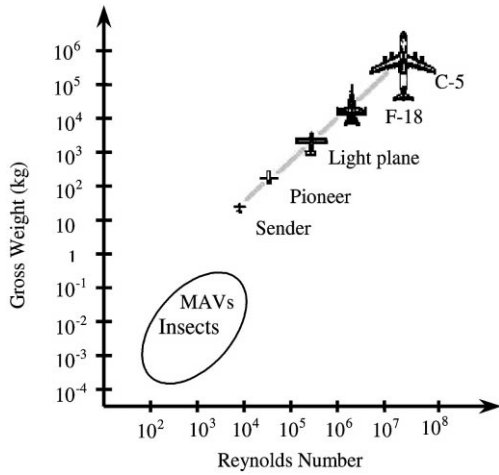


Fig. 1. MAV flight regime compared to existing flight vehicles [1].

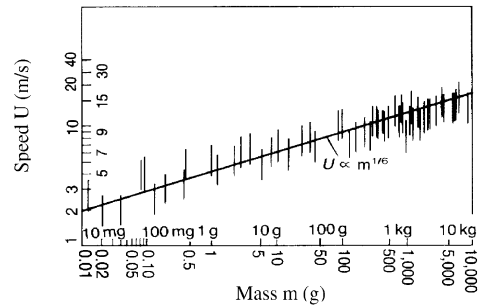


Fig. 3. Flight speed of birds [6].

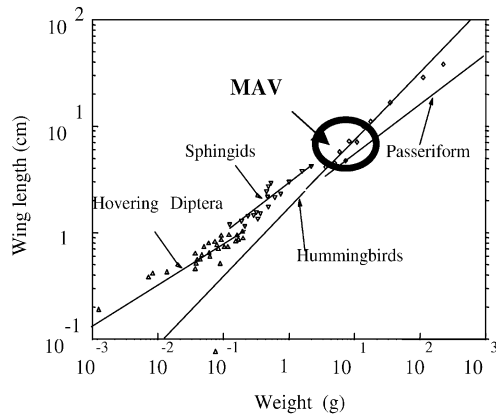


Fig. 2. Size of natural flyers.

natural flyers. We estimate that these flyers of MAV size with 15 cm wingspan weigh about 7–10 g. Thus, we believe that our ornithopter should weigh about the same.

Shown in Fig. 3 is statistical data on the speed versus size relationship from a wide range of birds [6]. The general

statistical tendency shows that the flight speed can be approximately given by

$$U = 4.77m^{1/6} \tag{1}$$

where  $U$  is the flight speed in m/s and  $m$  the mass in grams.

From statistical data on the wing flapping frequency versus the wing length [5], and wing flapping frequency versus mass [7] for birds and insects, a relationship of wingtip speed,  $U_{\text{vertical}}$ , and mass can be derived and are given by these following relations

$$U_{\text{vertical}}^{\text{upperbound}} = 11.7m^{-0.065} \tag{2}$$

$$U_{\text{vertical}}^{\text{lowerbound}} = 9.6m^{-0.043} \tag{3}$$

Combining Eqs. (1)–(3), a plot of wingtip speed and flight speed versus mass of insects and birds can be generated as shown in Fig. 4. The flight of flyers can be separated into two regimes: quasi-steady- and unsteady-states. For larger flyers, their flights can be approximated by quasi-steady-state assumptions because their wings flap at lower frequency during cruising. This means the wingtip speed is low compared to the flight speed. Thus, larger birds, such as eagles and seagulls, tend to have a soaring flight. Their wings behave closely to fixed-wings. On the other hand, smaller birds and insects fly in an unsteady-state regime in which their wingtip speed is faster than their flight speed, i.e. flies and mosquitoes flap their wings at several hundred

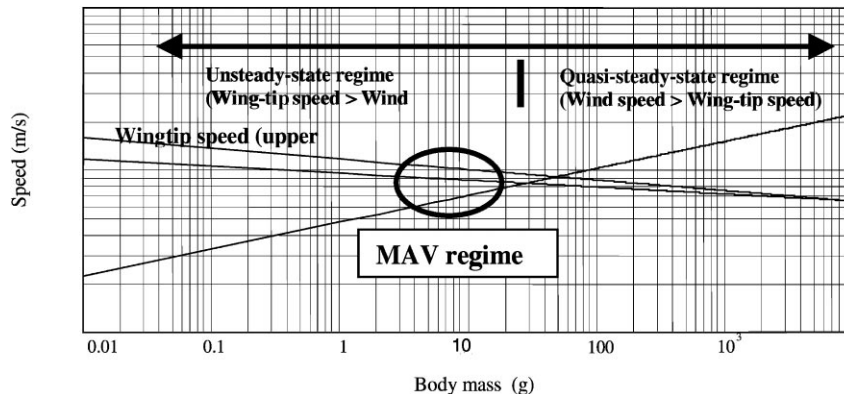


Fig. 4. Flight regime of steady- and unsteady-state of natural flyers.

hertz. From Fig. 4, we conclude that our MAV ornithopter (mass 7–10 g) operates in an unsteady-state flow regime in which the airflow over the wings is not constant over time and cannot be approximated by quasi-steady-state assumptions. During the unsteady-state flight, the airflow is separated from the wing at the leading edge and a separation “bubble” is formed during downstroke to generate a high lift coefficient during flight [8]. The vortex bubble is formed as the stagnation streamline rolls over the leading edge. This bubble continues to grow during the downstroke and is shed at the start of the upstroke.

Thus, one of the most difficult and challenging tasks is to design and develop a highly efficient wing that has an unsteady-state aerodynamic advantage. The wing must be light and strong. In addition, it also has to be able to withstand high flapping frequency without breaking and is capable of generating enough lift and thrust to fly the prototype vehicles.

## 2. Design and fabrication

We first built the model wings (non MEMS-based wings) using carbon fiber rods with 750 μm diameter as wing-frames. Thin mylar film and thin paper were glued to the carbon rod as wing membranes. These wings are shown in Fig. 5. However, we find that the method of making wings this way is cumbersome and there are several disadvantages. For example, glue adds weight and wings become too heavy. Moreover, an identical set of wings is difficult to achieve unless a mold is made for each fabrication. This is costly, time-consuming, and has a slow turn-around time, especially if the wing structure is complicated. This method cannot accommodate effectively and efficiently the study of the design variable changes.

For many reasons, we claim the new MEMS wing technology is necessary because MEMS wings enable systematic research in terms of repeatability, size control, weight minimization, mass production, and fast turn-around time. Moreover, complicated structures, such as dragonfly, butterfly, and beetle wings can be easily fabricated using photolithography technology.

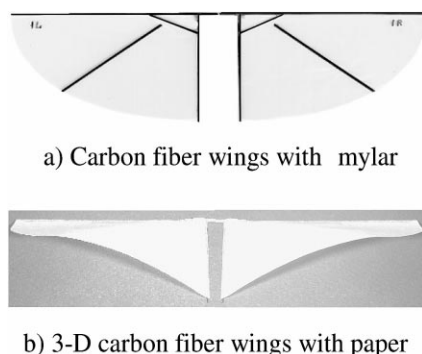


Fig. 5. Non MEMS-based wings.

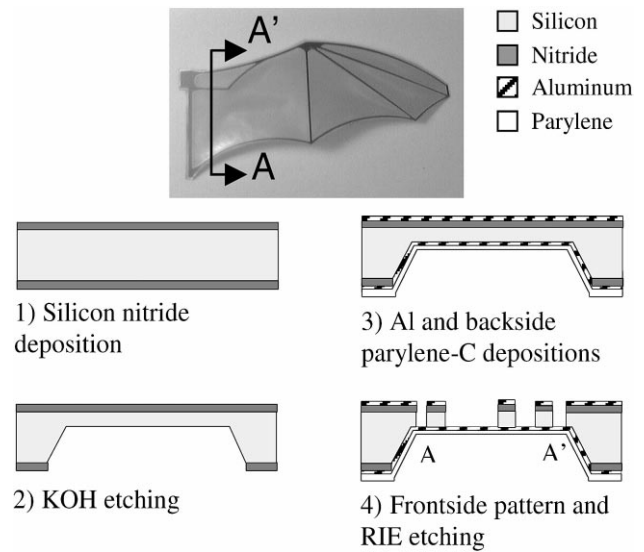


Fig. 6. Fabrication process of silicon MEMS wings.

Since our first approach is to learn from natural flyers and mimic them, we first designed our wings based on bat wings and other insect wings, such as beetle, butterfly, and dragonfly wings. We developed a MEMS fabrication process using silicon and parylene-C to make wingframes and membranes, respectively. The silicon wing fabrication process is shown in Fig. 6.

First, silicon nitride was deposited and patterned. It was used as a protecting mask during KOH etching. Then the silicon wafer was time-etched in KOH solution until 50 μm of diaphragm remained. Next, thin film aluminum was evaporated on both sides of the wafer and backside parylene-C deposition was performed. Then the frontside aluminum and nitride were patterned. They were used as a protecting mask during the RIE etching in order to form wingframes. Backside aluminum was used as an etch stop and to protect parylene-C membranes. The fabricated silicon bat and dragonfly wings are shown in Fig. 7. The bone width of the bat wing is 350 μm and the membrane thickness for both wings is 15 μm. Silicon wingframes, however, were too fragile. They broke easily. Therefore, we have developed an entirely new process using titanium-alloy metal as wingframes instead.

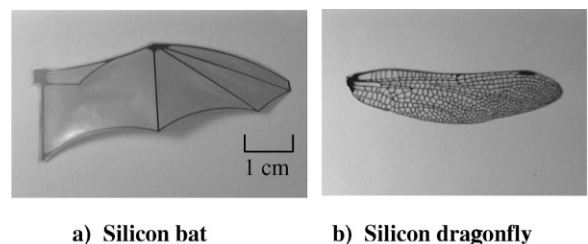


Fig. 7. MEMS fabricated silicon wings.

2.1. Titanium-alloy metal wings and parylene-C

We have experimented with various materials for wing-frame structures. Compared to titanium-alloy, these metals have several disadvantages. For example, aluminum metal is light in weight, but it is too soft. Stainless steel is strong, but its density is twice as high as that of titanium-alloy metal. The etchant solution for stainless steel, ferric chloride (FeCl<sub>3</sub>), is dark brown in color; it is almost impossible to see through during the etching process. Besides, it must be performed at a high temperature in order to yield a reasonable etching rate.

Ti-6Al-4V is the most widely commercially used titanium-alloy. It is composed of 88% titanium, 6% aluminum, 4% vanadium, and 2% of other elements, such as iron, carbon, hydrogen and oxygen. It is widely used for aircraft gas turbine disks and blades as well as airframe structural components that requires strength and high temperature tolerance. For this project, we have chosen titanium-alloy metal for several reasons. For example, it is light and strong and can be easily tapered to vary the thickness of wingspars. Because titanium-alloy is ductile, it also can be bent to create wing camber to improve performance. In addition, the etching process of titanium-alloy can be conducted at room temperature and yields a reasonable etching rate.

For wing membranes, we selected poly-monochloro-*para*-xylylene, or parylene-C [9]. Its chemical structure is shown in Fig. 8 [10]. The deposition takes place in a parylene deposition system model PDS 2010 Labcoter 1 from Specialty Coating Systems Inc. This system vaporizes the solid parylene-C dimer at 170°C. The pyrolysis takes place at 690°C. This will decompose the dimer at the two methylene–methylene bonds to yield stable monomers of monochloro-*para*-xylylene. When the monomers enter the deposition chamber, which is at room temperature, it condenses onto the substrate. The chamber size is 30.5 cm × 30.5 cm. The film deposited at these conditions is transparent and smooth with good uniformity. Depending on the coating surface area, 1 g of parylene-C dimer typically yields about 1 μm of thickness.

There are several advantages of using parylene-C as wing membrane: (1) it can be deposited directly onto titanium-alloy at any desired thickness; (2) its adhesion to titanium-alloy is excellent; (3) parylene film is light and strong, and can withstand high flapping frequency of more than 30 Hz without tearing and (4) parylene-C is deposited at room temperature and yields a conformal coating. Thus, step corners can be uniformly coated. Fig. 9 shows various fabricated titanium-alloy MEMS wings ranging from insect to simple spar wings. Table 1 shows selected

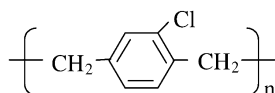


Fig. 8. Chemical structure of parylene-C.

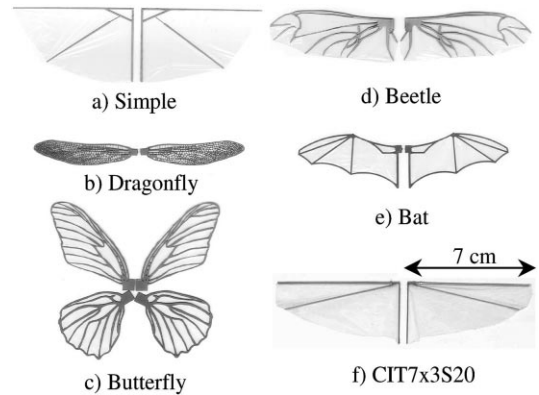


Fig. 9. Titanium-alloy MEMS wings.

Table 1  
Mechanical properties of Ti-6Al-4V [11] and parylene-C [10]

Properties	Ti-6Al-4V	Parylene-C
Density (g/cm <sup>3</sup> )	4.5	1.3
Young's modulus (GPa)	110	3
Tensile strength (MPa)	100	70
Yield strength (MPa)	97	56
Coefficient of thermal expansion (× 10 <sup>-5</sup> /°C)	0.9	3.5

mechanical properties of both titanium-alloy metal and parylene-C.

2.2. Titanium-alloy wing fabrication process

Fig. 10 shows the fabrication process of titanium-alloy MEMS wing.

First, a 250-μm-thick titanium-alloy substrate was cleaned in trichloroethylene (TCE) for 20 min. Later, it was dipped in a diluted HF solution to roughen its surface to improve the adhesion to the dry film resist. Next, the dry film resist was laminated on both sides of the substrate. The dry film resist (DFR-4713) and the dry film laminator

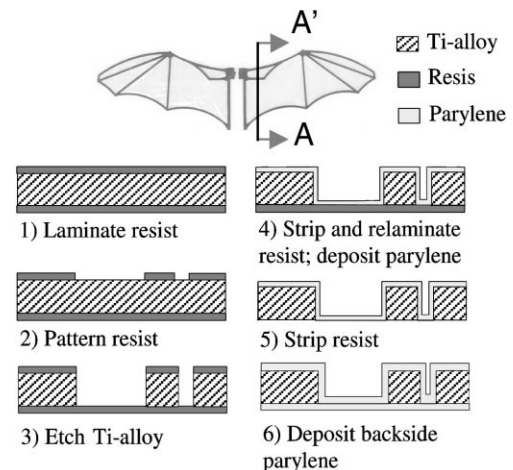


Fig. 10. Fabrication process of titanium-alloy MEMS wings.

(model BTL-121A) can be obtained from Kepro Circuit System Inc. [12]. The resist was patterned for 45 s under UV light and was developed in Na<sub>2</sub>CO<sub>3</sub> solution for 5–6 min. Then it was hardbaked at 120°C for 20 min. Next, the substrate was etched in a mixed solution of 5% HF and 2% HNO<sub>3</sub>. We found that if the concentration of the acid was too strong, the dry film resist would peel off before the etching was finished. At this concentration, the etching rate was about 2.5 μm/min. Because this was an isotropic etching, the undercut rate was about the same as etching rate. Therefore, undercut must be taken into a consideration during the mask design.

After the etching process was finished and the wingframes were formed, we stripped the resist from both sides of titanium-alloy substrate in a diluted KOH solution. Then the dry film resist was relaminated on the backside. It was used as a platform for parylene-C polymers to deposit upon. Next, parylene-C deposition was performed. Afterwards, dry film resist was stripped. This left clear membranes of parylene-C attached to the titanium-alloy wingframes. Finally, in order to strengthen the wing membrane, the second layer of parylene-C was deposited.

We found that having a right protective mask during etching was very important. One of the crucial fabrication steps was the release of a large area of wing without damaging the parylene-C membrane. The material chosen must be able to withstand HF and HNO<sub>3</sub> acids and could be stripped off easily without destroying the titanium-alloy metal and the parylene-C membranes. We selected negative dry film resist (DFR-4713) because it met these requirements. We also found that its adhesion to titanium-alloy substrate was good during etching even without any adhesion promoter. In addition, the resist was stripped off easily in a diluted KOH solution if the film was exposed under the UV light beforehand. Both titanium-alloy and parylene-C were not attacked by KOH at all.

### 3. Testing and results

#### 3.1. Mechanical testing

The wing stiffness test setup is shown in Fig. 11. The wing was clamped at its root. A blade, connected to a loadcell and an XYZ stage, was used to probe at various sections of the

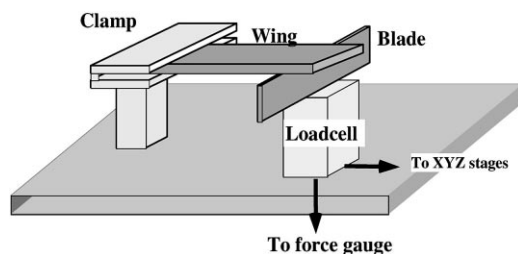


Fig. 11. Spring constant test setup schematic.

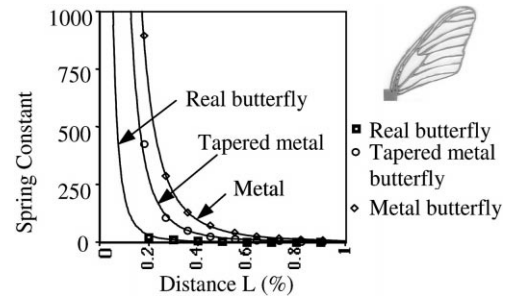


Fig. 12. Spring constant of butterfly wings.

wings to measure its stiffness. We see that MEMS wings can be tapered to vary thickness to mimic the natural wing's stiffness distribution. Tapering of MEMS wings can be achieved by selectively etching the wings in a diluted mixed solution of HF and HNO<sub>3</sub> acids. Tapered wing's stiffness, when normalized with weight, is also comparable to that of the natural wing. Fig. 12 shows the plot of the wing's spring constant versus normalized distance from wing's root of a butterfly wing. From this plot, we can obtain the relationship between the spring constant  $K$  of the butterfly wings, in N/m, to the normalized distance  $L$  from wing roots as follows:

$$K_{\text{real butterfly}} = 0.452L^{-2.663} \tag{4}$$

$$K_{\text{tapered metal butterfly}} = 7.73L^{-2.774} \tag{5}$$

$$K_{\text{metal butterfly}} = 2.775L^{-2.871} \tag{6}$$

From the relationship between the spring constant  $K$  of a cantilever beam of length  $L$ , we would expect that  $K$  is proportional to  $L^{-3}$  [13]. Eqs. (4)–(6) show similar results.

#### 3.2. Transmission design

We built a lightweight, low-friction transmission mechanism to convert the rotary motion of the driving motor into the flapping motion of the wings. Four transmission designs were considered and are shown in Fig. 13. Based on simplicity, minimal weight, and flapping symmetry, only

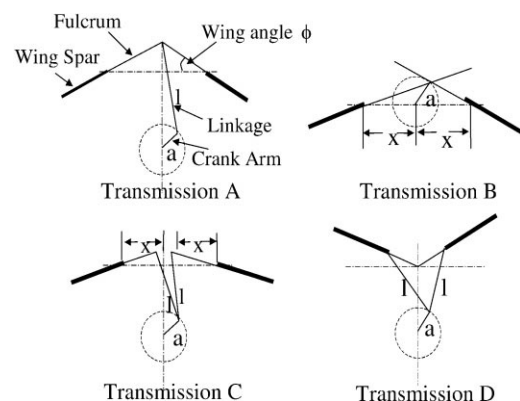


Fig. 13. Various transmission designs.

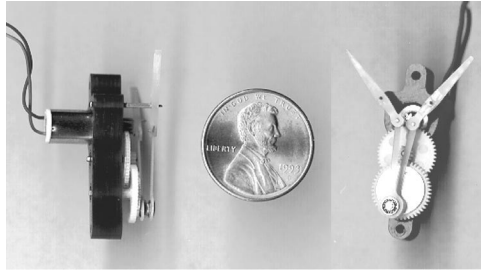


Fig. 14. Fabricated transmission C.

the design of transmission C was implemented and built as shown in Fig. 14. This design restricts the flapping motion in a plane perpendicular to the motor shaft. A small dc motor with gearbox ratio of 22:1 was used to drive the transmission. The maximum of 1.5 W can be used to drive this motor. At this power, with no wing attached, the transmission can flap up to 42 Hz continuously for a few minutes without destroying the motor. MEMS wings were then mounted on the transmission system and several flapping tests were performed. The wings could withstand more than 30 Hz of flapping. Neither breaking nor tearing of wing membrane was observed.

3.3. Wind tunnel test results

The MAV aerodynamic study was conducted at UCLA in a high quality low-speed wind tunnel with velocity uniformity of 0.5% and speeds from 1 to 10 m/s. The wind tunnel has a 30 cm × 30 cm × 60 cm test section with a 4:1 contraction. Force measurements were taken using low capacity 2-D force loadcells. This test setup is shown in Fig. 15.

The aerodynamic performance of natural insect wings, carbon fiber wings, and MEMS wings were studied. We first compared the natural wings to nature-mimic wings and studied the effect of flexibility of the leading edge. As shown in Fig. 16, wind tunnel test results show that spanwise stiffness is an important factor in lift production in flapping flight. For the same size of wings, cicada wings with rigid leading edges produce larger lift coefficients compared to our previous design of metal bat wings that have flexible leading edges.



a) Low-speed wind tunnel b) Force loadcells

Fig. 15. Wind tunnel test setup.

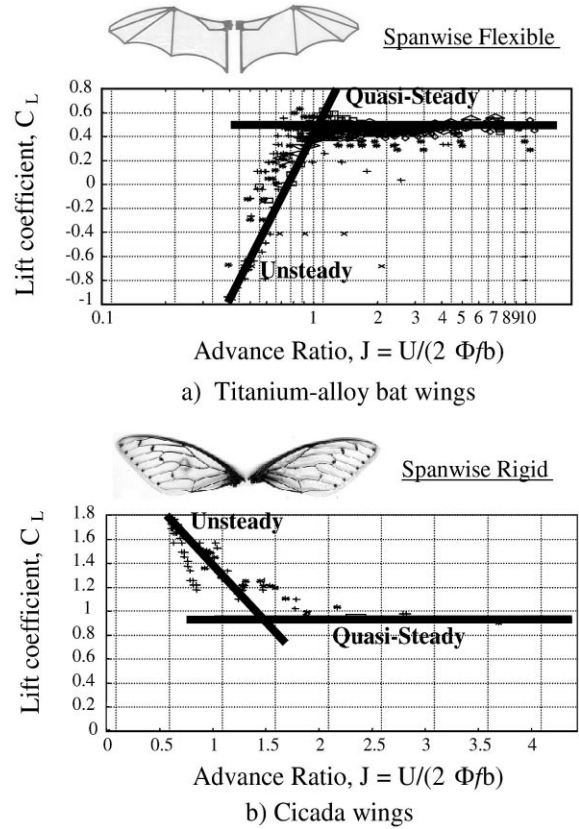


Fig. 16. Spanwise stiffness effect.

The lift and thrust coefficients can be expressed as follows:

$$C_L = \frac{2L}{\rho AU^2} \tag{7}$$

and

$$C_T = \frac{2T}{\rho AU^2} \tag{8}$$

where  $L$ ,  $T$ ,  $U$ ,  $A$ , and  $r$  are lift, thrust, flight speed, wing planform area, and air density, respectively. The advance ratio  $J$  is the ratio of the flight speed to the speed of the wingtip and is given by

$$J = \frac{U}{2\Phi fb} \tag{9}$$

where  $F$ ,  $f$ , and  $b$  are stroke angle, flapping frequency, and wing semi-span, respectively. Typically, unsteady-state flight has an advance ratio  $J$  of less than 1. For example, natural fliers such as bumblebee, black fly and fruit fly have an advance ratio in free flight of 0.66, 0.50 and 0.33, respectively [14].

Our wind tunnel test results show that nature-mimic MEMS wings with complicated structure performed poorly compared to the real wings. This is because the real wings are much lighter and more rigid. They also have 3-D shapes. Therefore, instead of trying to mimic the natural wings, we refocused our efforts in designing and fabricating simpler

Table 2  
Properties of various wing designs<sup>a</sup>

Wing types	A	B	C	D
Weight (each) (mg)	220	220	150	150
Frame material	C	C	Ti	Ti
Membrane material	myl	pap	par	par
Angle of diagonal spa (°)	45	n/a	10	20
Planform $L \times W$ (cm)	$7 \times 5$	$7 \times 3$	$7 \times 3$	$7 \times 3$

<sup>a</sup> C: carbon fiber rod; Ti: titanium-alloy; myl: mylar; pap: paper; par: parlylene-C; L: spanwise; W: chordwise.

wings that could generate enough lift and thrust to fly our prototypes. These wings are compared and listed in Table 2. Lift and thrust coefficients resulted from the wind tunnel test are shown in Fig. 17. Fig. 18 shows the input power required to flap these wings. Our current MEMS wing type D (CIT7 × 3S20) with rigid leading edge shows the best result in terms of lift, thrust, and power required among the rest. Using the motor we have, it only requires 1 W of power to flap at 30 Hz.

Compared to the paper wings, because CIT7 × 3S20 wings were fabricated by using MEMS technology, they are very light and can be batch-fabricated. They also require less input power to fly and can be actuated up to 30 Hz.

#### 4. Prototype vehicles

##### 4.1. Super capacitor-powered ornithopter

We built a super capacitor-powered electric motor free-flight ornithopter, shown in Fig. 19. This prototype weighs

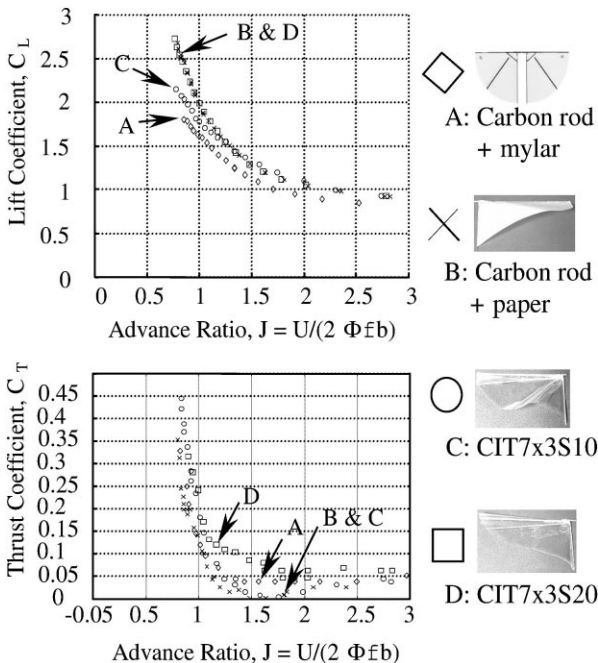


Fig. 17. Lift and thrust coefficients of various types of wings.

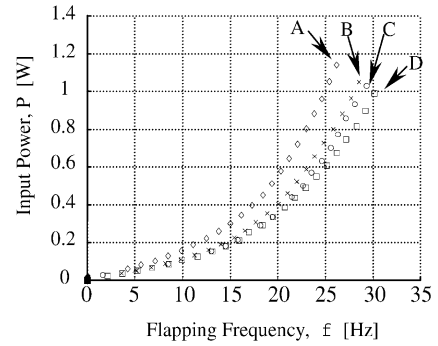


Fig. 18. Input power.

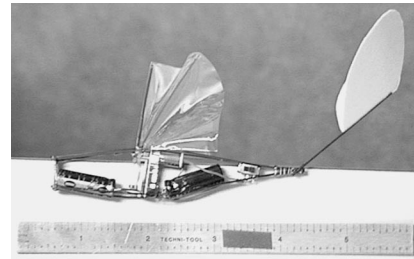


Fig. 19. Super capacitor-powered ornithopter.

only 6.5 g as shown in Table 3. The system is composed of an electric motor, a transmission system, two 1 F super capacitors, MEMS wings, a carbon-fiber-rod fuselage, and tail stabilizers. On the bench test, the flapping duration was less than a minute before having to recharge the capacitors. This is much shorter compared to the NiCd battery’s discharge time.

##### 4.2. Battery-powered ornithopter

Because the battery is a better power source compared to super capacitor, it is our desire to build a palm-sized battery-powered ornithopter MAV. This prototype is shown in Fig. 20. The fuselage was redesigned and super capacitors were replaced with a rechargeable NiCd battery and a dc-to-dc converter. The mass summary of the battery-powered ornithopter is shown in Table 4.

As the size of the flyers decreases, finding a powerful, yet light, power source has become one of the most difficult challenges. The lightest rechargeable battery available

Table 3  
Mass summary for super capacitor-powered ornithopter

Components	Weight (g)
MEMS wings	0.3
Motor and transmission system	2.4
Super capacitors	2.0
Fuselage, tail, switch, wires, etc.	1.8
Total weight	6.5

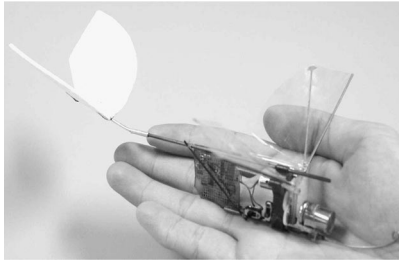


Fig. 20. Battery-powered ornithopter MAV.

Table 4  
Mass summary for battery-powered ornithopter

Components	Weight (g)
MEMS wings	0.3
Motor and transmission system	3.1
Battery	3.0
dc-to-dc Converter	1.9
Fuselage, tail, switch, wires, etc.	2.2
Total weight	10.5

found “off-the-shelf” in the market is Sanyo NiCd N-50. It weighs about 3.5 g. We trimmed the casing as thin as possible to reduce the weight to 3 g. Since the NiCd battery produces only 1 V nominally and the desired voltages to drive the motor is 4–6 V, a dc-to-dc converter was custom-built to step up the voltage to the necessary level. Fig. 21 shows discharge time for various output voltage settings of the converter. As the battery continues to discharge to a certain length of time, the voltage starts to drop. This will decrease the flapping frequency and the flight time.

This lightweight converter weighs only about 1.9 g. The voltage output is adjustable and can be set before each flight test. The advantage of the converter and a NiCd cell power system is that it is lightweight and takes advantage of the good specific power and energy of the 50 mA h NiCd cell. We cannot use a higher quantity of smaller batteries to deliver the same power and performance due to the weight constraint.

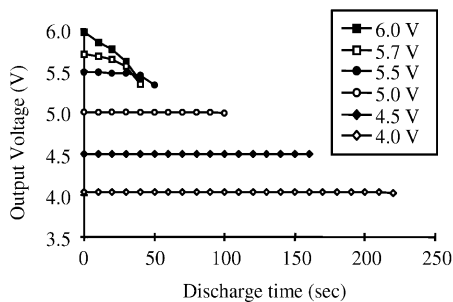


Fig. 21. Continuous discharge time for various output voltage settings of the dc-to-dc converter.

### 4.3. Flight test

Because we have not incorporated a radio control device in our prototypes, the flight will be an autonomous flight. We tested metal wings and carbon fiber wings with both ornithopters. During these free flight tests, the flyer gained and maintained the altitude at the beginning of the flight. Then it slowly descended after the power source was almost completely discharged. The lift generated was no longer able to support the weight of the vehicle. Flight durations of 5–18 s were achieved. So far, the best flight duration for the super capacitor-powered ornithopter was 9 and 18 s for the battery-powered ornithopter. The flight duration was mainly limited by the power system and vehicle’s weight. In both cases, the metal wings did not break during several landing crashes.

We find that there are several challenges in order to achieve a successful sustained flight. First, the wind condition must be perfect. Often during the flight test, the wind speed and direction shifted constantly. Second, the trim of tail stabilizer must be crucial. Finally, each launch motion must be the same. We also believe that our current wings and ornithopter are not yet optimized, thus we hope future flight duration can still be improved.

## 5. Future direction

There are several tasks that we plan to accomplish in the future. For a MAV at this size, though the weight constraint may have almost reached its limit for the current design, we hope to be able to further reduce the weight so that it can fly longer. However, because the incorporation of a radio control device is desired for the future prototypes, to accommodate a higher weight budget, a new design may have to be considered. This will be a challenging task. It may require a bigger motor, larger wings, and a new high-efficiency dc-to-dc converter in order to gain more lift and thrust. Furthermore, we plan to fabricate MEMS strain gauges onto the wings so that the wing loading can be measured. In addition, we also plan to fabricate a novel MEMS electrostatic membrane actuators onto the wings to selectively control their stiffness distribution.

## 6. Conclusions

A novel titanium-alloy wingframe technology has been developed for MEMS wings. Several MEMS wings were fabricated with parameters, such as chord and spar widths, membrane thickness, number of spars, and sweep angles, varied. We believe that only MEMS technology can easily and systematically accommodate these many variable changes with a fast turn-around time. Wind tunnel tests were performed in the high quality wind tunnel. These wings have been tested under cyclic conditions to assess long-term

reliability. Super capacitor-powered and battery-powered prototype MAVs were built and test-flown. The best free flight duration of 9 and 18 s were achieved by super capacitor-powered and battery-powered ornithopters, respectively.

### Acknowledgements

This work is supported under DARPA/TTO MAV program DABT63-98-C-0005. The authors would like to thank Dr. Sangwook Lee for his work in silicon-fabricated wings, Dr. Hany Nassef from UCLA for the wind tunnel testing, and Joel Grasmeyer and Matt Keennon at the MAV program, AeroVironment Inc.

### References

- [1] J.M. McMichael, M.S. Francis, Micro Air Vehicles — Toward a New Dimension in Flight, [http://www.darpa.mil/ttp/mav/mav\\_auvsi.html](http://www.darpa.mil/ttp/mav/mav_auvsi.html) (1997).
- [2] M. Okamoto, K. Yasuda, A. Azuma, Aerodynamic characteristics of the wings and body of a dragonfly, *J. Exp. Biol.* 199 (1996) 281–294.
- [3] M. Sato, A. Azuma, The flight performance of a Damselfly *Ceriatrigon Melanurum Selys*, *J. Exp. Biol.* 200 (1997) 1765–1779.
- [4] M.F.M. Osborne, Aerodynamic of flapping flight with application to insects, *J. Exp. Biol.* 28 (1951) 221–245.
- [5] C.H. Greenewalt, Dimensional relationships for flying animals, *Smithsonian Miscellaneous Collections* 144 (2) (1962) 1–46.
- [6] C.J. Pennycuik, The mechanics of bird migration, *IBIS* 3 (1969) 525–556.
- [7] A. Azuma, *The Biokinetics of Flying and Swimming*, Springer, Tokyo, 1992.
- [8] G.R. Spedding, *Adv. Comparative Environ. Phys.* 11 (1992) 51–111.
- [9] J.T.C. Yeh, K.R. Grebe, Patterning of poly-*para*-xylylenes by reactive ion etching, *J. Vacuum Sci. Technol. A* 1 (2) (1983) 604–608.
- [10] Parylene Conformal Coatings Specifications and Properties, Specialty Coating Systems Inc., 5707 West Minnesota Street, Indianapolis, IN.
- [11] *Metal Handbook*, 9th Edition, Vol. 3, American Society for Metals, Cleveland, OH, 1980, pp. 388–391.
- [12] Kepro Circuit Systems Inc., 3640 Scarlet Oak Blvd., St. Louis, MO.
- [13] S. Timoshenko, G.H. MacCullough, *Elements of Strength of Materials*, 3rd Edition, Van Nostrand, New York, 1949.
- [14] S. Vogel, *Life in Moving Fluids*, 2nd Edition, Princeton University Press, Princeton, 1994.